

Existence of Hebel-Slichter peak in unconventional kagome superconductors

Yi Dai, Andreas Kreisel, and Brian M. Andersen

Niels Bohr Institute, University of Copenhagen, DK-2200 Copenhagen, Denmark

(Dated: October 17, 2024)

We perform a theoretical investigation of the spin susceptibility of unconventional superconductivity on the kagome lattice. Despite the existence of a sign-changing gap structure, which sums to zero over the Fermi surface, we show that such unconventional pairing states may exhibit a Hebel-Slichter peak in the temperature-dependent spin-lattice relaxation rate. It originates from destructive sublattice interference effects. For the same reason, unconventional pairing states on the kagome lattice tend not to exhibit a neutron resonance peak. These results supplement previous theoretical studies of the surprising robustness of sign-changing gap structures to disorder on the kagome lattice. Taken together these findings imply that unconventional superconductivity on the kagome lattice is deceptive in the sense that its properties may appear similar to conventional non-sign-changing superconductivity. These results may be of relevance to the superconducting state of the kagome superconductors AV_3Sb_5 (A : K, Rb, Cs) and $CsTi_3Bi_5$.

I. INTRODUCTION

For progress in the understanding of unconventional superconductivity it is crucial to experimentally determine the nature of the superconducting ground state. This is a demanding collective task that requires agreement between a vast range of different experimental probes. Pinpointing the pairing state includes determination of the spin structure of the Cooper pairs and their relative spatial dependence, i.e. the realized irreducible representation of the associated crystal point group [1–3]. Together these properties hold valuable clues to the dominant fluctuations driving the Cooper pairing [4–8]. In this endeavor, it is important to identify any possible sign changes of the gap function, which is experimentally challenging as most probes are insensitive to the phase of the superconducting order parameter. An exception is scattering off impurities or sample edges which does allow for access to the phase. Likewise, two-particle correlation functions can be phase sensitive as evidenced for example by the spin susceptibility featuring a Hebel-Slichter peak in the nuclear magnetic resonance (NMR) spin-lattice relaxation rate, and the neutron resonance peak detected by inelastic neutron scattering experiments. We return to a discussion of these signatures further below, demonstrating that for the kagome lattice the phase-sensitiveness is wiped out by destructive sublattice interference effects.

In recent years, the discussion of possible unconventional superconductivity on the kagome lattice has been motivated by the discovery of superconductivity in vanadium-based kagome metals AV_3Sb_5 (A : K, Rb, Cs) [9–11]. The kagome lattice is particularly interesting since the associated band structure exhibits a flat band, van Hove singularities, and Dirac points, as seen in Fig. 1. Importantly, the distribution of sublattice weights of the eigenstates on the Fermi surface, also illustrated in Fig. 1c, plays an important role in determining the leading instabilities arising from interactions [12–15]. This may be relevant for the AV_3Sb_5 materials where superconductivity appears in proxim-

ity to a charge-density wave phase [16–27]. For the superconducting phase, theoretical studies have explored Cooper pairing arising both from purely electronic fluctuations [12, 21, 22, 24, 28–35] and via the importance of phonon contributions [36–41]. From pairing via spin- and charge-fluctuations, the E_2 irreducible representation with d -wave (or $d \pm id$) pairing symmetry stands out as a leading candidate [32].

Experimentally, the nature of the superconducting ground state in the AV_3Sb_5 compounds remains unresolved at present [42], with conflicting evidence for both standard nodeless non-sign-changing gaps and nodal unconventional superconducting order [19, 43–47]. A Knight shift suppression and the existence of a Hebel-Slichter peak below T_c in the spin-lattice relaxation rate measured by NMR experiments were interpreted as evidence for s -wave spin-singlet superconductivity [48]. This agrees with recent laser ARPES measurements reporting isotropic (momentum-independent) spectroscopic gaps [49]. Penetration depth data and specific heat measurements on CsV_3Sb_5 have been analysed in terms of an anisotropic, but non-sign-changing gap with a finite small minimum gap [10, 50–53]. Reference 52 measured electron irradiation effects on the penetration depth and found no evidence for disorder-generated low-energy density of states enhancements, as expected from sign-changing gap functions. Likewise, a non-sign-changing gap function appears consistent with the absence of in-gap bound states near nonmagnetic impurities [44] and a weak dependence of the critical transition temperature T_c on the residual resistivity ratio (sample quality) [54].

Indeed, the response of superconductivity to disorder can play an important role in determining the nature of superconductivity since it typically acts as a phase-sensitive probe [55–59]. Disorder effects can be studied both from the possible generation of impurity bound states detectable by local probes and an overall disorder-averaged response verified by thermodynamic probes or transport measurements. When nonmagnetic disorder generates in-gap bound states or if it strongly reduces T_c ,

it is traditionally a strong indicator of an unconventional superconducting condensate. These conclusions about the effects of disorder on unconventional sign-changing gap structures are, however, partly invalidated on the kagome lattice. As recently demonstrated, the sublattice weight of the band eigenstates play a crucial role for determining the response of superconductivity to disorder on the kagome lattice [60]. Specifically, even though the unconventional gap function averages to zero over the Fermi surface, $\sum_{\mathbf{k}} \Delta(\mathbf{k}) = 0$, atomic-scale disorder only scatters to a limited allowed region of the Fermi surface. For even-parity (spin-singlet) superconductivity this has important consequences, including the absence of in-gap bound states and a slow T_c -suppression rate [60]. In this light, unconventional (spin-singlet) superconductivity on the kagome lattice is protected from nonmagnetic disorder, a fact that may be of importance for the interpretation of several of the experiments mentioned above [44, 52, 54].

In this paper we study the spin susceptibility in the superconducting state on the kagome lattice within a minimal tight-binding model. Based on the evidence for spin-singlet Cooper pairs, we focus on the spin-lattice relaxation rate in the even-parity states: A_1 (s -wave) and E_2 (d -wave) superconducting order. Surprisingly, despite a fully compensated sign-changing gap structure, the relaxation rate exhibits a pronounced Hebel-Slichter peak upon entering the superconducting state. In addition, the neutron resonance peak expected for sign-changing gap structures is largely wiped out [61–65]. The origin of these effects can be traced to the peculiar properties of the matrix elements from sublattice to band space on the kagome lattice. Thus, in short, unconventional spin-singlet superconductivity on the kagome lattice takes the deceptive appearance of a conventional superconductor. This conclusion is in line with the unusual disorder effects mentioned above [60]. Our results lead to a reconsideration of the superconducting state of kagome superconductors under current investigations, and specifically invalidates the conclusion that a Hebel-Slichter peak implies conventional s -wave superconductivity for these compounds.

II. BASIC BAND STRUCTURE OF THE KAGOME LATTICE

The minimal tight-binding model of electronic states on the kagome lattice is shown in Fig. 1. The Hamiltonian of the tight-binding model is given by

$$\mathcal{H}_0 = \sum_{\mathbf{k}, \sigma} \psi_{\mathbf{k}\sigma}^\dagger H_0(\mathbf{k}) \psi_{\mathbf{k}\sigma}, \quad (1)$$

where $\psi_{\mathbf{k}\sigma} = (c_{\mathbf{k}\sigma A} \ c_{\mathbf{k}\sigma B} \ c_{\mathbf{k}\sigma C})^T$ and

$$H_0(\mathbf{k}) = - \begin{pmatrix} \mu & t \cos k_3 & t \cos k_1 \\ t \cos k_3 & \mu & t \cos k_2 \\ t \cos k_1 & t \cos k_2 & \mu \end{pmatrix}. \quad (2)$$

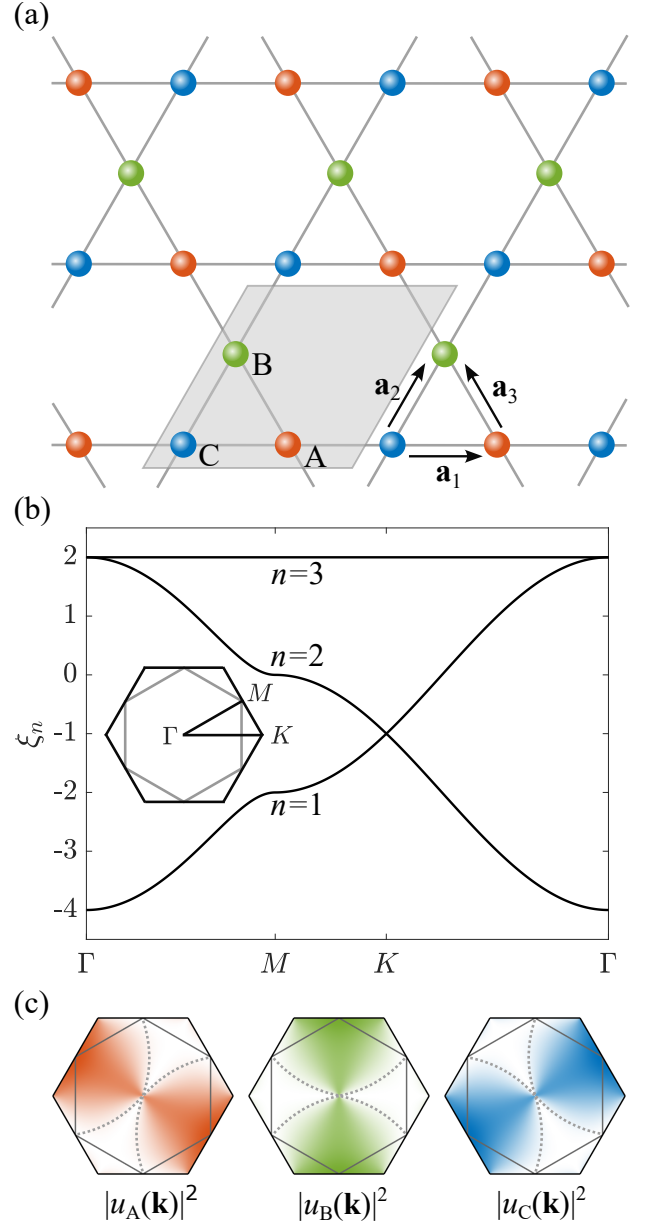


FIG. 1. (a) Illustration of the kagome lattice with sublattice vectors \mathbf{a}_n . (b) Energy bands of the tight-binding model $\xi_n(\mathbf{k})$ in units of t along the path shown in the inset. The dark gray lines inside in the Brillouin zone (BZ) define the Fermi surface at $\mu = 0$. (c) Distribution of the sublattice weights across the BZ for the middle band ($n = 2$). The colors refer to the same sublattices shown in (a). The dashed lines sketch the area where the sublattice weights are zero.

Here $k_n = \mathbf{k} \cdot \mathbf{a}_n$, where $\mathbf{a}_1 = \frac{1}{2} (1 \ 0)$, $\mathbf{a}_2 = \frac{1}{2} (\frac{1}{2} \ \frac{\sqrt{3}}{2})$ and $\mathbf{a}_3 = \frac{1}{2} (-\frac{1}{2} \ \frac{\sqrt{3}}{2})$. μ refers to the chemical potential, we use the NN hopping integrals $t = 1$ as energy unit in the following. The Hamiltonian is diagonalized by a unitary transformation, $u_{n\alpha}^*(\mathbf{k}) H_{0,\alpha\beta}(\mathbf{k}) u_{\beta m}(\mathbf{k}) = \xi_n(\mathbf{k}) \delta_{nm}$ yielding the band energies $\xi_n(\mathbf{k})$ and the eigenstates

$u_{n\alpha}(\mathbf{k})$ of band n . The resulting band structure is shown in Fig. 1(b) and features a Dirac point at the K point and two van Hove singularities at the M point. In addition, for the nearest-neighbor (NN) tight-binding model there is a flat band that acquires dispersion upon including further neighbor hoppings. The kagome lattice is endowed with a property which has become known as sublattice interference [12] for which specific hopping trajectories interfere destructively and result in electronic wavefunctions that localize on specific sites inside the unit cell. Specifically, electronic states at the upper van Hove singularity, at $\mu = 0$, are localized on only one of the three sublattice sites in the unit cell, as illustrated in Fig. 1(c). By contrast, states at the lower van Hove singularity near $\mu = -2$ localize on two of the three sublattice sites.

III. SPIN-LATTICE RELAXATION RATE

A. Revisiting the one-band square lattice

In order to set the stage for the discussion of the superconducting spin susceptibility on the kagome lattice, we start by briefly revisiting basic properties of the spin susceptibility in the superconducting state on the square lattice. In that case, the bare retarded BCS spin susceptibility $\chi_0^{+-}(\mathbf{q}, \omega)$ at momentum \mathbf{q} and frequency ω is given by

$$\chi_0^{+-}(\mathbf{q}, \omega) = \frac{1}{\mathcal{N}} \sum_{\mathbf{k}, E > 0} \left[\left(1 - \frac{\xi_{\mathbf{k}} \xi_{\mathbf{k}+\mathbf{q}} + \Delta_{\mathbf{k}+\mathbf{q}}^* \Delta_{\mathbf{k}}}{E_{\mathbf{k}} E_{\mathbf{k}+\mathbf{q}}} \right) \frac{1 - f(E_{\mathbf{k}}) - f(E_{\mathbf{k}+\mathbf{q}})}{\omega + E_{\mathbf{k}+\mathbf{q}} + E_{\mathbf{k}} + i\eta} + \left(1 - \frac{\xi_{\mathbf{k}} \xi_{\mathbf{k}+\mathbf{q}} + \Delta_{\mathbf{k}+\mathbf{q}}^* \Delta_{\mathbf{k}}}{E_{\mathbf{k}} E_{\mathbf{k}+\mathbf{q}}} \right) \frac{f(E_{\mathbf{k}}) + f(E_{\mathbf{k}+\mathbf{q}}) - 1}{\omega - E_{\mathbf{k}+\mathbf{q}} - E_{\mathbf{k}} + i\eta} \right. \\ \left. + \left(1 + \frac{\xi_{\mathbf{k}} \xi_{\mathbf{k}+\mathbf{q}} + \Delta_{\mathbf{k}+\mathbf{q}}^* \Delta_{\mathbf{k}}}{E_{\mathbf{k}} E_{\mathbf{k}+\mathbf{q}}} \right) \frac{f(E_{\mathbf{k}}) - f(E_{\mathbf{k}+\mathbf{q}})}{\omega + E_{\mathbf{k}+\mathbf{q}} - E_{\mathbf{k}} + i\eta} + \left(1 + \frac{\xi_{\mathbf{k}} \xi_{\mathbf{k}+\mathbf{q}} + \Delta_{\mathbf{k}+\mathbf{q}}^* \Delta_{\mathbf{k}}}{E_{\mathbf{k}} E_{\mathbf{k}+\mathbf{q}}} \right) \frac{f(E_{\mathbf{k}+\mathbf{q}}) - f(E_{\mathbf{k}})}{\omega + E_{\mathbf{k}} - E_{\mathbf{k}+\mathbf{q}} + i\eta} \right], \quad (3)$$

where \mathcal{N} denotes the number of points summed over in the Brillouin zone (BZ), and η is an infinitesimal positive factor arising from the analytical continuation. Additionally, $\xi_{\mathbf{k}}$ is the electron dispersion, $\Delta_{\mathbf{k}}$ the superconducting order parameter, $E_{\mathbf{k}} = \sqrt{\xi_{\mathbf{k}}^2 + |\Delta_{\mathbf{k}}|^2}$ denotes the energy of superconducting quasiparticles, and $f(E_{\mathbf{k}})$ is the Fermi-Dirac distribution function. Because of the Nambu particle-hole symmetry, we can sum only over positive $E_{\mathbf{k}}$.

The spin-lattice relaxation rate is related to the imaginary part of spin susceptibility $\chi_0^{+-}(\mathbf{q}, \omega)$ by [66, 67]

$$\alpha \equiv \frac{1}{T_1 T} \propto \lim_{\omega \rightarrow 0} \frac{1}{\mathcal{N}} \sum_{\mathbf{q}} \text{Im} \frac{\chi_0^{+-}(\mathbf{q}, \omega)}{\omega}. \quad (4)$$

The tight-binding model of the square lattice is

$$\mathcal{H}_0 = \sum_{\mathbf{k}\sigma} [-2t(\cos k_x + \cos k_y) - \mu] c_{\mathbf{k}\sigma}^\dagger c_{\mathbf{k}\sigma}. \quad (5)$$

For the purpose of illustration, we consider two distinct superconducting cases: (1) a conventional isotropic s -wave order parameter $\Delta_{\mathbf{k}}^s = \Delta_0 = 0.2$, and (2) a sign-changing d -wave order parameter given by $\Delta_{\mathbf{k}}^d = \frac{\Delta_0}{2}(\cos k_x - \cos k_y)$. In Eq. (3), only the last two terms can give non-zero values for the imaginary part in the superconducting states in the limit $\omega \rightarrow 0$ [68]. In addition to a sharp onset of the order parameter at T_c , the factors in the associated brackets

$$\left(1 + \frac{\xi_{\mathbf{k}} \xi_{\mathbf{k}+\mathbf{q}} + \Delta_{\mathbf{k}+\mathbf{q}}^* \Delta_{\mathbf{k}}}{E_{\mathbf{k}} E_{\mathbf{k}+\mathbf{q}}} \right), \quad (6)$$

are key to the existence of a Hebel-Slichter peak. We can illustrate this by defining a factor

$$B(\mathbf{q}, \mathbf{k}_n) = \frac{\Delta_{\mathbf{k}_n+\mathbf{q}}^* \Delta_{\mathbf{k}_n}}{E_{\mathbf{k}_n} E_{\mathbf{k}_n+\mathbf{q}}}, \quad (7)$$

where \mathbf{k}_n is a \mathbf{k} -point on the Fermi surface, here chosen by the point that gives the largest contribution to $\chi_0^{+-}(\mathbf{q}, \omega)$. Figure 2 shows that $\sum_{\mathbf{q}} B(\mathbf{q}, \mathbf{k}_n)$ is a finite value between 0 and 1 in the s -wave case, which enhances $\chi_0^{+-}(\mathbf{q}, \omega)$ and contributes to a Hebel-Slichter peak, as seen from Fig. 3. By contrast, for the d -wave case it gives no enhancement because the positive and negative contributions cancel, as evident from Fig. 2. Consequently, as is well-known, there is essentially no Hebel-Slichter peak for the d -wave order parameter as seen from Fig. 3 [69].

B. The kagome lattice

Superconductivity on the kagome lattice can be described through the usual Nambu formalism

$$\mathcal{H} = \sum_{\mathbf{k}} \Psi_{\mathbf{k}}^\dagger \hat{H}(\mathbf{k}) \Psi_{\mathbf{k}}, \quad (8)$$

where

$$\hat{H}(\mathbf{k}) = \begin{pmatrix} H_0(\mathbf{k}) & -\Delta(\mathbf{k}) \\ -\Delta(\mathbf{k})^\dagger & -H_0^T(-\mathbf{k}) \end{pmatrix}, \quad (9)$$

and $\Psi_{\mathbf{k}}^\dagger = (c_{\mathbf{k}\uparrow}^\dagger \ c_{-\mathbf{k}\downarrow})$ with $c_{\mathbf{k}\sigma}^\dagger = (c_{\mathbf{k}\sigma A}^\dagger \ c_{\mathbf{k}\sigma B}^\dagger \ c_{\mathbf{k}\sigma C}^\dagger)$. For on-site (OS) Cooper pairing, the superconducting order parameters with A_1 (s -wave), and E_2 ($d_{x^2-y^2}$ - and

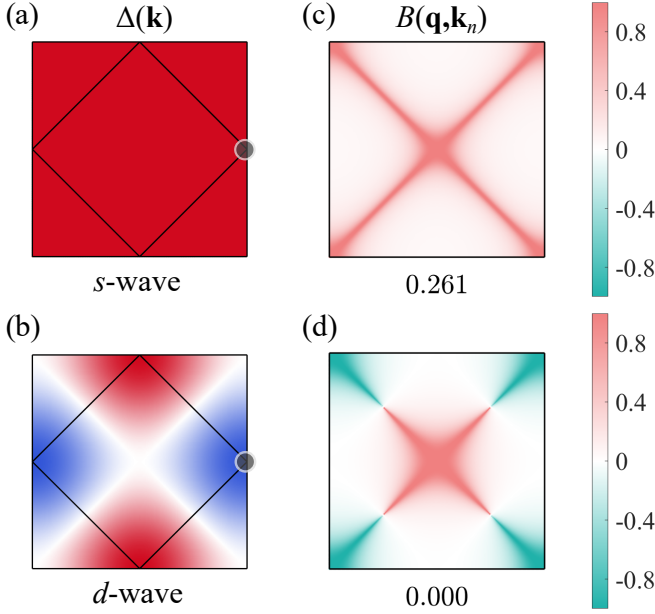


FIG. 2. Panels (a) and (b) display the s -wave and $d_{x^2-y^2}$ -wave order parameters in \mathbf{k} -space in the first BZ for the square lattice. The black lines indicate the Fermi surface at $\mu = 0$. Panels (c) and (d) display $B(\mathbf{q}, \mathbf{k}_n)$ defined in Eq. (7) in \mathbf{q} -space for the s -wave and $d_{x^2-y^2}$ -wave order parameters, respectively. The chosen momentum point \mathbf{k}_n is shown by the black dot in (a) and (b). The numbers below (c) and (d) indicate the sum $\sum_{\mathbf{q}} B(\mathbf{q}, \mathbf{k}_n)$.

d_{xy} -wave) symmetries are [60]

$$\Delta_{\Gamma} = \Delta_0 f_{\text{OS},\Gamma}, \quad (10)$$

where

$$f_{\text{OS},s} = \frac{1}{\sqrt{3}} \begin{pmatrix} +1 & 0 & 0 \\ 0 & +1 & 0 \\ 0 & 0 & +1 \end{pmatrix}, \quad (11)$$

$$f_{\text{OS},d_{x^2-y^2}} = \frac{1}{\sqrt{6}} \begin{pmatrix} +1 & 0 & 0 \\ 0 & -2 & 0 \\ 0 & 0 & +1 \end{pmatrix}, \quad (12)$$

$$f_{\text{OS},d_{xy}} = \frac{1}{\sqrt{2}} \begin{pmatrix} +1 & 0 & 0 \\ 0 & 0 & 0 \\ 0 & 0 & -1 \end{pmatrix}. \quad (13)$$

The $d_{x^2-y^2}$ and d_{xy} orders belonging to the 2D E_2 irreducible representation can also be obtained via NN pairing. These harmonics, however, are zero on the Fermi surface near the upper van Hove point [32, 60, 70], and since only states close to the Fermi surface contribute to the imaginary part of the spin susceptibility $\text{Im} \chi_0^{+-}(\mathbf{q}, \omega)$, NN pairing terms lead to small contributions and are not important for the results presented here. The main feature in the kagome lattice due to the sublattice interference in the normal state band structure is bound to the symmetry of the order parameter. Since all higher harmonics of the order parameter belong to

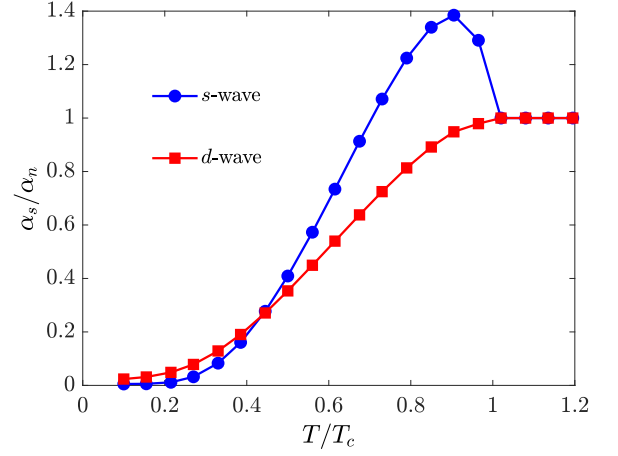


FIG. 3. Temperature dependence of the spin-lattice relaxation rate ratio α_s/α_n for the simple square lattice. Here, α_s and α_n denote the relaxation rates $1/T_1 T$ of the superconducting state and normal states, respectively. All cases are plotted for $N = 4 \times 10^4$ and $\omega = \eta = 0.015$. As seen, the sign-changing gap of the $d_{x^2-y^2}$ form wipes out the Hebel-Slichter peak.

the same irrep, these are also subject to the same effects. Hence, we only show the on-site d -wave pairing terms. Additionally, below we will also address the time-reversal symmetry breaking superposition $d + id$ defined by

$$\Delta_{d+id} = \frac{\Delta_0}{\sqrt{2}} (f_{\text{OS},d_{x^2-y^2}} + i f_{\text{OS},d_{xy}}), \quad (14)$$

which is expected to be the preferred solution at sufficiently low temperatures T within the E_2 irreducible representation. In the following, we set $\Delta_0 = 0.2$.

We can apply the unitary transformation that diagonalizes H_0 to transform the order parameter from sublattice space to band space

$$\Delta_{nm}(\mathbf{k}) = u_{n\alpha}^*(\mathbf{k}) \Delta_{\alpha\beta} u_{m\beta}^*(-\mathbf{k}), \quad (15)$$

where $u_{n\alpha}(\mathbf{k})$ is the eigenstate of $H_0(\mathbf{k})$ in band n . Since only the middle band ($n = m = 2$) crosses the Fermi surface near the upper van Hove point at $\mu = 0$, we can ignore interband pairing and use an effective Hamiltonian with solely this band

$$H_{\text{eff}}(\mathbf{k}) = \begin{pmatrix} \xi_2(\mathbf{k}) & -\Delta_{22}(\mathbf{k}) \\ -\Delta_{22}^*(\mathbf{k}) & -\xi_2(\mathbf{k}) \end{pmatrix}. \quad (16)$$

In Appendix A, we show that this approximation agrees well with the numerical result obtained from the full Hamiltonian $\hat{H}(\mathbf{k})$. For simplicity, we use the notation $\xi_{\mathbf{k}} \equiv \xi_2(\mathbf{k})$ and $\Delta_{\mathbf{k}} \equiv \Delta_{22}(\mathbf{k})$ in the following expressions. The spin susceptibility of the kagome lattice is

$$\chi_0^{+-}(\mathbf{q}, \tau) = \frac{1}{N^2} \sum_{\substack{\mathbf{k}\mathbf{k}' \\ \alpha\beta}} \langle T_{\tau} c_{\alpha,\mathbf{k}+\mathbf{q}}^{\dagger} c_{\alpha,\mathbf{k}} c_{\beta,\mathbf{k}'}^{\dagger} c_{\beta,\mathbf{k}'+\mathbf{q}}(\tau) c_{\beta,\mathbf{k}'}(\tau) \rangle. \quad (17)$$

In order to simplify this expression, we can perform the transformation from sublattice to band space. In band space, the approximation that only the middle band is

chosen can further simplify it. Additionally, by performing a Fourier transformation, the spin susceptibility can be written in the frequency domain

$$\chi_0^{+-}(\mathbf{q}, \omega) = \frac{1}{\mathcal{N}} \sum_{\mathbf{k}, E > 0} \left[\left(1 - \frac{\xi_{\mathbf{k}} \xi_{\mathbf{k}+\mathbf{q}} + \Delta_{\mathbf{k}+\mathbf{q}}^* \Delta_{\mathbf{k}}}{E_{\mathbf{k}} E_{\mathbf{k}+\mathbf{q}}} \right) \frac{1 - f(E_{\mathbf{k}}) - f(E_{\mathbf{k}+\mathbf{q}})}{\omega + E_{\mathbf{k}+\mathbf{q}} + E_{\mathbf{k}} + i\eta} + \left(1 - \frac{\xi_{\mathbf{k}} \xi_{\mathbf{k}+\mathbf{q}} + \Delta_{\mathbf{k}+\mathbf{q}}^* \Delta_{\mathbf{k}}}{E_{\mathbf{k}} E_{\mathbf{k}+\mathbf{q}}} \right) \frac{f(E_{\mathbf{k}}) + f(E_{\mathbf{k}+\mathbf{q}}) - 1}{\omega - E_{\mathbf{k}+\mathbf{q}} - E_{\mathbf{k}} + i\eta} \right. \\ \left. + \left(1 + \frac{\xi_{\mathbf{k}} \xi_{\mathbf{k}+\mathbf{q}} + \Delta_{\mathbf{k}+\mathbf{q}}^* \Delta_{\mathbf{k}}}{E_{\mathbf{k}} E_{\mathbf{k}+\mathbf{q}}} \right) \frac{f(E_{\mathbf{k}}) - f(E_{\mathbf{k}+\mathbf{q}})}{\omega + E_{\mathbf{k}+\mathbf{q}} - E_{\mathbf{k}} + i\eta} + \left(1 + \frac{\xi_{\mathbf{k}} \xi_{\mathbf{k}+\mathbf{q}} + \Delta_{\mathbf{k}+\mathbf{q}}^* \Delta_{\mathbf{k}}}{E_{\mathbf{k}} E_{\mathbf{k}+\mathbf{q}}} \right) \frac{f(E_{\mathbf{k}+\mathbf{q}}) - f(E_{\mathbf{k}})}{\omega + E_{\mathbf{k}} - E_{\mathbf{k}+\mathbf{q}} + i\eta} \right] \sum_{\alpha\beta} g_{\alpha\beta}(\mathbf{k}, \mathbf{q}), \quad (18)$$

which is the same expression as for the square lattice, except for an extra factor $\sum_{\alpha\beta} g_{\alpha\beta}(\mathbf{k}, \mathbf{q})$ arising from the transformation from sublattice to band space with

$$g_{\alpha\beta}(\mathbf{k}, \mathbf{q}) = u_{2\alpha}(\mathbf{k} + \mathbf{q}) u_{2\beta}(\mathbf{k} + \mathbf{q}) u_{2\alpha}(\mathbf{k}) u_{2\beta}(\mathbf{k}). \quad (19)$$

We can write the eigenvectors without considering complex conjugation because they are real under the basis choice in Eq. (2). For the kagome lattice, it is customary to use another basis that is periodic in the first BZ. As discussed in Appendix B, care must be exerted for obtaining the spin susceptibility in that basis.

Similar to the discussion of the square lattice, we can define a (dressed) spin-susceptibility coherence factor given by

$$B_d(\mathbf{q}, \mathbf{k}_n) = \frac{\sum_{\alpha\beta} g_{\alpha\beta}(\mathbf{k}_n, \mathbf{q}) \Delta_{\mathbf{k}_n+\mathbf{q}}^* \Delta_{\mathbf{k}_n}}{Z E_{\mathbf{k}_n} E_{\mathbf{k}_n+\mathbf{q}}}, \quad (20)$$

where Z is a normalization factor defined by

$$Z = \frac{1}{\mathcal{N}^2} \sum_{\mathbf{k}, \mathbf{q}} \sum_{\alpha\beta} g_{\alpha\beta}(\mathbf{k}, \mathbf{q}). \quad (21)$$

For comparison, we also define a bare coherence factor without the matrix element dressing from $g_{\alpha\beta}(\mathbf{k}, \mathbf{q})$

$$B_b(\mathbf{q}, \mathbf{k}_n) = \frac{\Delta_{\mathbf{k}_n+\mathbf{q}}^* \Delta_{\mathbf{k}_n}}{E_{\mathbf{k}_n} E_{\mathbf{k}_n+\mathbf{q}}}. \quad (22)$$

In Fig. 4 we show both the bare and dressed coherence factors for the s - and d -wave pairing states on the kagome lattice. Considering first the A_1 s -wave case seen in Fig. 4(a,d,g), even though the dressing factor $g_{\alpha\beta}(\mathbf{k}, \mathbf{q})$ changes the distribution of $B_b(\mathbf{q}, \mathbf{k}_n)$ in \mathbf{q} -space, the summed value $\sum_{\mathbf{q}} B_d(\mathbf{q}, \mathbf{k}_n)$ remains substantial and unchanged. Therefore, the corresponding $1/T_1 T$ curve remains the same in both the bare and dressed cases of s -wave superconductivity, both exhibiting a Hebel-Slichter peak as expected, see Fig. 5.

By contrast, for the d -wave case the dressing factor $g_{\alpha\beta}(\mathbf{k}, \mathbf{q})$ originating from the sublattice to band space transformation becomes crucial, as seen from comparing Fig. 4(e,f) to Fig. 4(h,i). There we compare the coherence factors $B_b(\mathbf{q}, \mathbf{k}_n)$ and $B_d(\mathbf{q}, \mathbf{k}_n)$ for the two \mathbf{k} -points

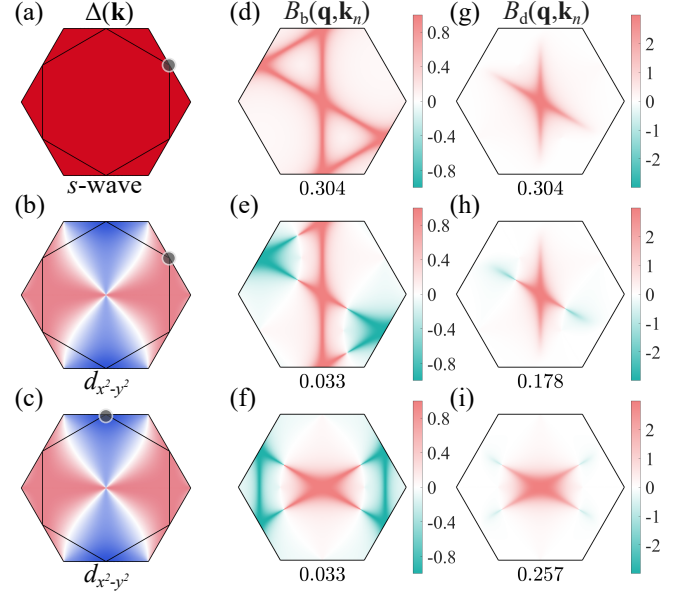


FIG. 4. The s -wave order parameter (a) and the $d_{x^2-y^2}$ order parameter (b)-(c) in \mathbf{k} -space in the first BZ for the kagome lattice. The black lines indicate the Fermi surface at $\mu = 0$. Panel (d) displays the bare $B_b(\mathbf{q}, \mathbf{k}_n)$ [Eq. (22)] for the s -wave order parameter in \mathbf{q} -space and panels (e)-(f) are for the $d_{x^2-y^2}$ order parameter. Panel (g) displays the dressed $B_d(\mathbf{q}, \mathbf{k}_n)$ [Eq. (20)] in \mathbf{q} -space for the s -wave order parameters and panels (h)-(i) are for the $d_{x^2-y^2}$ order parameter. The chosen \mathbf{k}_n for (d)-(i) is indicated by the black dots in (a)-(c) in the same row. The numbers below (d)-(f) and (g)-(i) display the summed values $\sum_{\mathbf{q}} B_b(\mathbf{q}, \mathbf{k}_n)$ and $\sum_{\mathbf{q}} B_d(\mathbf{q}, \mathbf{k}_n)$, respectively.

highlighted in Fig. 4(b,c). Evidently, $g_{\alpha\beta}(\mathbf{k}, \mathbf{q})$ destroys the compensation (the near cancellation between positive and negative regions) seen in Fig. 4(e,f) and leads to substantial summed values of $\sum_{\mathbf{q}} B_d(\mathbf{q}, \mathbf{k}_n)$, as seen from Fig. 4(h,i). The origin of this effect is tied to the sublattice weights. More specifically, for the second band the sublattice weights vanish identically on extended regions of the BZ as seen from Fig. 1 (c). For the d -wave order parameters, the sign changes occur between regions of largest weight and regions with zero weight. Therefore,

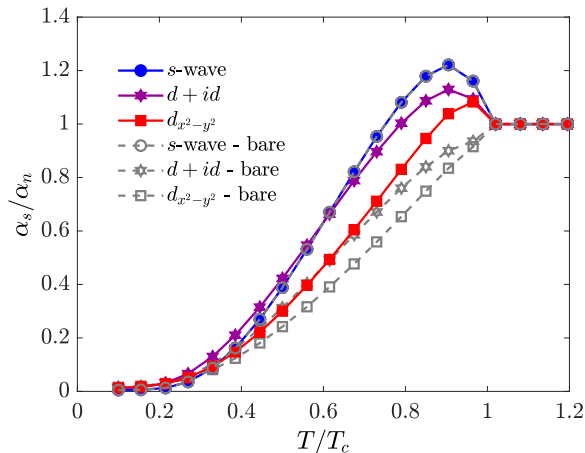


FIG. 5. Temperature dependence of the spin-lattice relaxation rate ratio α_s/α_n for superconductivity on the kagome lattice. All cases are plotted for $\mathcal{N} = 4 \times 10^4$ and $\omega = \eta = 0.015$. The solid lines show the results calculated from the full $\chi_0^{+-}(\mathbf{q}, \omega)$, while the dashed lines display the results obtained from the spin susceptibility without the dressing factor $g_{\alpha\beta}(\mathbf{k}, \mathbf{q})$. As seen, $g_{\alpha\beta}(\mathbf{k}, \mathbf{q})$ restores the Hebel-Slichter peak even for the d -wave cases.

most of the sign change in the gap function is “washed out” by the product of the components of the eigenvectors in Eq. (19). This conclusion is based on symmetry and therefore is not qualitatively altered if further neighbor pairing terms are present in the system, which we explicitly checked in separate calculations. This implies that while the bare d -wave case should not exhibit a Hebel-Slichter peak, the full (dressed) case should. Indeed, as seen from Fig. 5 this is the case. As a result, there exists a pronounced Hebel-Slichter peak in the case of d -wave superconductivity on the kagome lattice. This is the main result of the present paper. This conclusion is both valid for the nodal d -wave cases and the nodeless TRSB $d + id$ order. For the $d + id$ case, $\sum_{\mathbf{q}} B_d(\mathbf{q}, \mathbf{k}_n)$ remains real, even though the order parameter itself is complex. This is further discussed in Appendix C.

As seen from Fig. 4, the summed values $\sum_{\mathbf{q}} B_d(\mathbf{q}, \mathbf{k}_n)$ are smaller in the dressed d -wave cases as compared to the s -wave case, resulting in slightly smaller Hebel-Slichter peaks in d -wave cases. This, however, is only a quantitative difference, with the important point being that, unlike the bare case or d -wave order on the square lattice, the Hebel-Slichter peak is not wiped out despite the sign-changing gap. In summary, because of the kagome sublattice structure, which appears as the dressing factor $g_{\alpha\beta}(\mathbf{k}, \mathbf{q})$, the enhancement factor $\sum_{\mathbf{q}} B_d(\mathbf{q}, \mathbf{k}_n)$ in $\chi_0^{+-}(\mathbf{q}, \omega)$ becomes substantial and d -wave superconductivity supports a Hebel-Slichter peak on the kagome lattice, as seen from Fig. 5.

We note that the measurements of the NMR relaxation rate were done using Sb nuclear spins which are located in between the V atoms in the crystal structure. In this case the coupling between the nuclear spins and the con-

duction electrons is not a contact interaction and form factors appear in Eq. (4). We derive these explicitly in Appendix D and show that the qualitative conclusions are not altered by the additional form factor weighting of the momentum structure of the susceptibility.

IV. DISCUSSION AND CONCLUSIONS

We have demonstrated the existence of a Hebel-Slichter peak in the spin-lattice relaxation rate for d -wave superconductivity on the kagome lattice, and explained its existence from cancellation effects due to the peculiar sublattice-to-band space matrix elements. This result remains qualitatively unchanged if the system is (i) slightly away from the the upper van Hove filling, or (ii) if further neighbor pairing terms are present. However, if band 1 forms the Fermi surface with the mixed-type sublattice structure, the sublattice weights do not vanish anywhere in the BZ, and the kagome system behaves as an ordinary superconductor. In this case, unconventional pairing states do not exhibit a Hebel-Slichter peak. This result is in line with previous theoretical studies of the robustness of sign-changing gap structures to disorder on the kagome lattice [60]. Another example of unusual response is exemplified by the neutron resonance peak [61–65], i.e. a collective resonant spin state inside the 2Δ gap of the spin susceptibility at some pronounced scattering vector \mathbf{q} , that depends on the band structure at hand. For the neutron resonance peak, it is the first two terms of Eqs. (3) and (18) that are important. Therefore the relevant coherence factor is given by

$$\left(1 - \frac{\xi_{\mathbf{k}} \xi_{\mathbf{k}+\mathbf{q}} + \Delta_{\mathbf{k}+\mathbf{q}}^* \Delta_{\mathbf{k}}}{E_{\mathbf{k}} E_{\mathbf{k}+\mathbf{q}}}\right), \quad (23)$$

highlighting the absence (presence) of a neutron resonance mode for momentum vectors \mathbf{q} connecting same-sign (opposite-sign) gap regions. For the kagome lattice, the factor $g_{\alpha\beta}(\mathbf{k}, \mathbf{q})$ will significantly reduce contributions coming from $\Delta_{\mathbf{k}+\mathbf{q}}^* \Delta_{\mathbf{k}}$ even though \mathbf{q} connect opposite signs of the gap. Therefore, the superconducting susceptibility is not expected to be significantly enhanced compared to the normal state, and in this sense the neutron resonance peak is wiped out.

Similar unusual properties may be expected in other correlation functions for crystal structures where the important contributing states exhibit pronounced sublattice differentiation. For the kagome lattice, important effects of the matrix elements may be expected also for, for example, the behavior of the penetration depth and thermal conductivity since these quantities are obtained from two-particle correlation functions.

At present, it remains an open question what is the relevance of the findings in the present paper to the AV_3Sb_5 (A: K, Rb, Cs) and $CsTi_3Bi_5$ kagome superconductors under intense current investigations. To the best of our knowledge, these materials may turn out to host conventional s -wave superconductivity despite their many

other unusual electronic properties [42]. However, the results in this paper, combined with Ref. [60], highlight the somewhat deceptive behavior of unconventional superconductivity on the kagome lattice, rendering it “conventional” in appearance. Specifically, *d*-wave superconductivity exhibits a Hebel-Slichter peak, no pronounced neutron resonance mode, and very weak T_c -suppression in response to nonmagnetic disorder. Therefore, from this perspective, the question of the pairing symmetry of the above-mentioned kagome superconductors remains open at present.

ACKNOWLEDGMENTS

We acknowledge fruitful discussions with M. H. Christensen, P. J. Hirschfeld and S. C. Holbæk. A.K. ac-

knowledges support by the Danish National Committee for Research Infrastructure (NUFI) through the ESS-Lighthouse Q-MAT.

Appendix A: Three-band model without approximation

Apart from performing the sublattice-to-band transformation shown in Eqs. (15) and (16), which results in the dressing factor $g_{\alpha\beta}(\mathbf{k}, \mathbf{q})$, one can also numerically diagonalize the BdG Hamiltonian Eq. (9) in sublattice space directly. The matrix that diagonalizes $\hat{H}(\mathbf{k})$ through $\mathbf{U}^{-1}(\mathbf{k})\hat{H}(\mathbf{k})\mathbf{U}(\mathbf{k})$ is

$$\mathbf{U}(\mathbf{k}) = \begin{pmatrix} u_{A,1,\mathbf{k}}^* & u_{A,2,\mathbf{k}}^* & u_{A,3,\mathbf{k}}^* & -v_{A,1,\mathbf{k}} & -v_{A,2,\mathbf{k}} & -v_{A,3,\mathbf{k}} \\ u_{B,1,\mathbf{k}}^* & u_{B,2,\mathbf{k}}^* & u_{B,3,\mathbf{k}}^* & -v_{B,1,\mathbf{k}} & -v_{B,2,\mathbf{k}} & -v_{B,3,\mathbf{k}} \\ u_{C,1,\mathbf{k}}^* & u_{C,2,\mathbf{k}}^* & u_{C,3,\mathbf{k}}^* & -v_{C,1,\mathbf{k}} & -v_{C,2,\mathbf{k}} & -v_{C,3,\mathbf{k}} \\ v_{A,1,\mathbf{k}}^* & v_{A,2,\mathbf{k}}^* & v_{A,3,\mathbf{k}}^* & u_{A,1,\mathbf{k}} & u_{A,2,\mathbf{k}} & u_{A,3,\mathbf{k}} \\ v_{B,1,\mathbf{k}}^* & v_{B,2,\mathbf{k}}^* & v_{B,3,\mathbf{k}}^* & u_{B,1,\mathbf{k}} & u_{B,2,\mathbf{k}} & u_{B,3,\mathbf{k}} \\ v_{C,1,\mathbf{k}}^* & v_{C,2,\mathbf{k}}^* & v_{C,3,\mathbf{k}}^* & u_{C,1,\mathbf{k}} & u_{C,2,\mathbf{k}} & u_{C,3,\mathbf{k}} \end{pmatrix}, \quad (\text{A1})$$

which can be obtained numerically. The spin susceptibility in this basis is

$$\begin{aligned} \chi_0^{+-}(\mathbf{q}, \omega) = & \frac{1}{\mathcal{N}} \sum_{\substack{\mathbf{k}, m, m' \\ \alpha\beta}} \left[(v_{\alpha,m,\mathbf{k}+\mathbf{q}}^* v_{\beta,m,\mathbf{k}+\mathbf{q}} u_{\alpha,m',\mathbf{k}}^* u_{\beta,m',\mathbf{k}} - v_{\alpha,m,\mathbf{k}+\mathbf{q}}^* u_{\beta,m,\mathbf{k}+\mathbf{q}} u_{\alpha,m',\mathbf{k}}^* v_{\beta,m',\mathbf{k}}) \frac{1 - f(E_{\mathbf{k}+\mathbf{q},m}) - f(E_{\mathbf{k},m'})}{\omega + E_{\mathbf{k}+\mathbf{q},m} + E_{\mathbf{k},m'} + i\eta} \right. \\ & + (u_{\alpha,m,\mathbf{k}+\mathbf{q}} u_{\beta,m,\mathbf{k}+\mathbf{q}}^* u_{\alpha,m',\mathbf{k}}^* u_{\beta,m',\mathbf{k}} + u_{\alpha,m,\mathbf{k}+\mathbf{q}}^* v_{\beta,m,\mathbf{k}+\mathbf{q}} u_{\alpha,m',\mathbf{k}}^* v_{\beta,m',\mathbf{k}}) \frac{f(E_{\mathbf{k}+\mathbf{q},m}) - f(E_{\mathbf{k},m'})}{\omega + E_{\mathbf{k},m'} - E_{\mathbf{k}+\mathbf{q},m} + i\eta} \\ & + (v_{\alpha,m,\mathbf{k}+\mathbf{q}}^* v_{\beta,m,\mathbf{k}+\mathbf{q}} v_{\alpha,m',\mathbf{k}}^* v_{\beta,m',\mathbf{k}} + v_{\alpha,m,\mathbf{k}+\mathbf{q}}^* u_{\beta,m,\mathbf{k}+\mathbf{q}} v_{\alpha,m',\mathbf{k}}^* u_{\beta,m',\mathbf{k}}) \frac{f(E_{\mathbf{k},m'}) - f(E_{\mathbf{k}+\mathbf{q},m})}{\omega + E_{\mathbf{k}+\mathbf{q},m} - E_{\mathbf{k},m'} + i\eta} \\ & \left. + (u_{\alpha,m,\mathbf{k}+\mathbf{q}} u_{\beta,m,\mathbf{k}+\mathbf{q}}^* v_{\alpha,m',\mathbf{k}}^* v_{\beta,m',\mathbf{k}} - u_{\alpha,m,\mathbf{k}+\mathbf{q}}^* v_{\beta,m,\mathbf{k}+\mathbf{q}} v_{\alpha,m',\mathbf{k}}^* u_{\beta,m',\mathbf{k}}) \frac{f(E_{\mathbf{k}+\mathbf{q},m}) + f(E_{\mathbf{k},m'}) - 1}{\omega - E_{\mathbf{k}+\mathbf{q},m} - E_{\mathbf{k},m'} + i\eta} \right]. \quad (\text{A2}) \end{aligned}$$

There is no approximation in this expression. We compare the results obtained from two methods in Fig. S1. As seen, they are very similar despite the approximation made in Eq. (16) that only considers the middle band relevant at the Fermi level. The result from the complete model is slightly larger than the effective model because of small contributions of the other bands. Thus, the Hebel-Slichter peak is larger in the complete model compared to the effective model.

Appendix B: Basis choice and associated phase factors

The Hamiltonian in Eq. (2) is not periodic in the first BZ, meaning that while the eigenvalues are periodic, the

eigenvectors are not. We can remedy this issue by choosing the size of the \mathbf{k} -grid twice that of the first BZ. Alternatively, we can apply the unitary transformation $T^{-1}(\mathbf{k})H_0(\mathbf{k})T(\mathbf{k})$, where

$$T(\mathbf{k}) = \begin{pmatrix} e^{-ik_1} & 0 & 0 \\ 0 & e^{-ik_2} & 0 \\ 0 & 0 & 1 \end{pmatrix}, \quad (\text{B1})$$

and the Hamiltonian matrix in the new basis becomes

$$\tilde{H}_0(\mathbf{k}) = - \begin{pmatrix} \mu & t(1+e^{2ik_3}) & t(1+e^{-2ik_1}) \\ t(1+e^{-2ik_3}) & \mu & t(1+e^{-2ik_2}) \\ t(1+e^{2ik_1}) & t(1+e^{2ik_2}) & \mu \end{pmatrix}, \quad (\text{B2})$$

which is periodic in the first BZ. The Nambu Hamiltonian can also be transformed to the new basis by

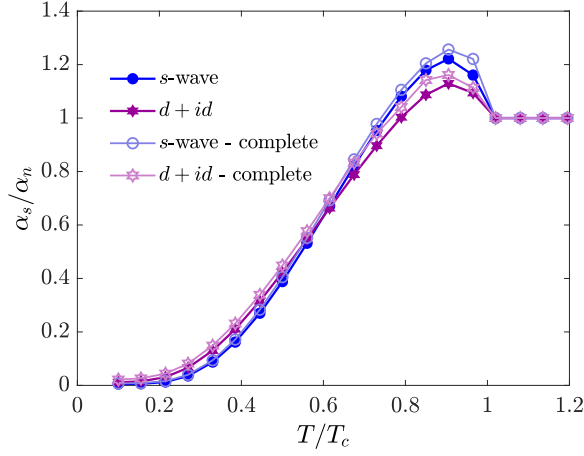


FIG. S1. Comparison of calculation including all bands (“complete”, Eq. (A2)) with the single band approximation, Eq. (18). The temperature dependence of the spin-lattice relaxation rate ratio α_s/α_n for the kagome system does only exhibit minor qualitative differences from the single-band approximation. Calculation for the single band approximation is done for $\mathcal{N} = 4 \times 10^4$ and the complete calculation for $\mathcal{N} = 1 \times 10^4$, respectively; $\omega = \eta = 0.015$ is used in both cases. The blue and purple lines show the results calculated from the effective Hamiltonian $H_{\text{eff}}(\mathbf{k})$. The respective lines with open symbols show the results obtained from the complete three-band Hamiltonian $\hat{H}(\mathbf{k})$.

$T_{\text{Nambu}}^{-1}(\mathbf{k})\hat{H}(\mathbf{k})T_{\text{Nambu}}(\mathbf{k})$, where

$$T_{\text{Nambu}}(\mathbf{k}) = \begin{pmatrix} T(\mathbf{k}) & 0 \\ 0 & T^T(-\mathbf{k}) \end{pmatrix}. \quad (\text{B3})$$

This transformation introduces extra phase factors in the spin susceptibility. We can recover the susceptibility under basis Eq. (2) by considering the phase factors

$$\chi_{0,\alpha\beta}^{+-}(\mathbf{q}, \omega) = \begin{pmatrix} \tilde{\chi}_{0,AA}^{+-} & e^{i(q_2 - q_1)} \tilde{\chi}_{0,AB}^{+-} & e^{-iq_1} \tilde{\chi}_{0,AC}^{+-} \\ e^{iq_1} \tilde{\chi}_{0,BA}^{+-} & \tilde{\chi}_{0,BB}^{+-} & e^{-iq_2} \tilde{\chi}_{0,BC}^{+-} \\ e^{iq_1} \tilde{\chi}_{0,CA}^{+-} & e^{iq_2} \tilde{\chi}_{0,CB}^{+-} & \tilde{\chi}_{0,CC}^{+-} \end{pmatrix}, \quad (\text{B4})$$

where $\tilde{\chi}_{0,\alpha\beta}^{+-}(\mathbf{q}, \omega)$ is the spin susceptibility in the new basis, and $q_n = \mathbf{q} \cdot \mathbf{a}_n$.

It is straightforward to use the basis in Eq. (2) for spin susceptibility calculations, while direct use of the basis Eq. (B2) breaks, for example, the C_2 symmetry by a rotation of π around the principal axis. As shown in Fig. S2(a), the spin susceptibility for sublattice index AB calculated from the basis in Eq. (2) is invariant under a C_2 rotation, which is a symmetry of the Hamiltonian. Figure S2(b) shows that the basis Eq. (B2) breaks this symmetry because the negative and positive parts cannot be mapped onto each other by this symmetry operation. However, by including the phase factors of Eq. (B4) one recovers the correct susceptibility. This symmetry breaking by an inappropriate choice of basis is also discussed in Ref. [71].

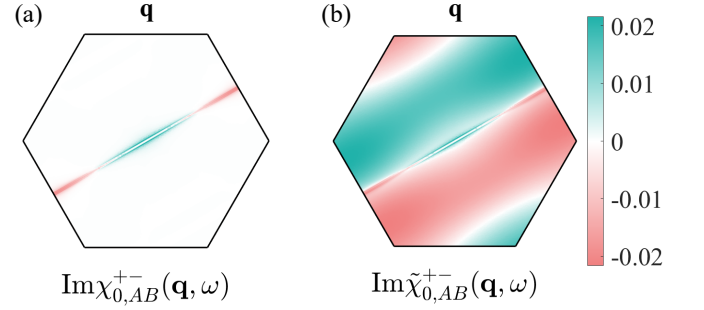


FIG. S2. Panel (a) displays $\text{Im} \chi_{0,AB}^{+-}(\mathbf{q}, \omega)$ with the basis Eq. (2). Panel (b) displays $\text{Im} \tilde{\chi}_{0,AB}^{+-}(\mathbf{q}, \omega)$ with the basis choice of Eq. (B2). (a) conserves the C_2 symmetry by a rotation of π around the principal axis; (b) breaks this symmetry.

Appendix C: Absence of imaginary part of B factor

For $d + id$ superconductivity, Δ_{d+id} is a complex number. Thus, in principle, the imaginary part of $B(\mathbf{q}, \mathbf{k})$ might contribute to $\chi_0^{+-}(\mathbf{q}, \omega)$. If only the real part of $B(\mathbf{q}, \mathbf{k})$ contributes to $\chi_0^{+-}(\mathbf{q}, \omega)$, then only the imaginary part of the Fermi function term, which is only non-zero near the Fermi surface, contributes to the imaginary part of $\chi_0^{+-}(\mathbf{q}, \omega)$. We define

$$\Delta_{\mathbf{k}} = \Delta'_{\mathbf{k}} + i\Delta''_{\mathbf{k}}, \quad (\text{C1})$$

where $\Delta'_{\mathbf{k}}$ and $\Delta''_{\mathbf{k}}$ denote the real and imaginary parts of $\Delta_{\mathbf{k}}$. Both $\Delta'_{\mathbf{k}}$ and $\Delta''_{\mathbf{k}}$ have the time-reversal symmetry, while $\Delta_{\mathbf{k}}$ breaks the time-reversal symmetry. $B(\mathbf{q}, \mathbf{k})$ can be written as

$$B(\mathbf{q}, \mathbf{k}) = \frac{(\Delta'_{\mathbf{k}+\mathbf{q}} - i\Delta''_{\mathbf{k}+\mathbf{q}})(\Delta'_{\mathbf{k}} + i\Delta''_{\mathbf{k}})}{E_{\mathbf{k}}E_{\mathbf{k}+\mathbf{q}}}, \quad (\text{C2})$$

and the imaginary part is

$$\text{Im} B(\mathbf{q}, \mathbf{k}) = \frac{\Delta'_{\mathbf{k}+\mathbf{q}}\Delta''_{\mathbf{k}} - \Delta''_{\mathbf{k}+\mathbf{q}}\Delta'_{\mathbf{k}}}{E_{\mathbf{k}}E_{\mathbf{k}+\mathbf{q}}}. \quad (\text{C3})$$

Since we sum over \mathbf{k} in $\chi_0^{+-}(\mathbf{q}, \omega)$, we can do $\mathbf{k} \rightarrow -\mathbf{k} - \mathbf{q}$ for the first term of Eq. (C3). Due to the even parity property $\Delta'_{\mathbf{k}} = \Delta'_{-\mathbf{k}}$, $\Delta''_{\mathbf{k}} = \Delta''_{-\mathbf{k}}$ and $E_{\mathbf{k}} = E_{-\mathbf{k}}$ together, the imaginary part gives zero. Thus for Δ_{d+id} , we can still only consider $\text{Re} B(\mathbf{q}, \mathbf{k})$.

Appendix D: Form factors

The general expression for the NMR relaxation rate is derived from perturbation theory [66, 72]. The perturbation is described by the hyperfine coupling interaction

$$\mathcal{H}_{\text{hf}} = \sum_i \mathbf{I} \cdot \bar{\mathbf{A}}_i \cdot \mathbf{S}_{i\alpha}, \quad (\text{D1})$$

where \mathbf{I} and $\mathbf{S}_{i\alpha}$ denote the nuclear and electron spins. The index i labels the sites to which the nuclear spin

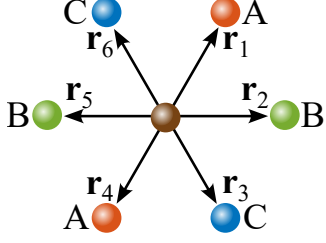


FIG. S3. Illustration of the in-plane antimony atom in the kagome superconductors AV_3Sb_5 . The brown site refers to the antimony atom, and the colored ones refer to the vanadium atoms on three different sublattice sites.

couples. In the case of V NMR, it is sufficient to consider only the onsite term, while for Sb NMR, the sum runs over the nearest neighbor V atoms where conducting electrons couple to the nuclear spin as shown in Fig. S3. The index α labels the corresponding sublattice indices on those sites. $\bar{\mathcal{A}}_i$ is the hyperfine coupling matrix describing the coupling between the nuclear and electron spins, which can be written in Cartesian coordinates as

$$\bar{\mathcal{A}}_i = \begin{pmatrix} \mathcal{A}_i^{xx} & \mathcal{A}_i^{xy} & \mathcal{A}_i^{xz} \\ \mathcal{A}_i^{yx} & \mathcal{A}_i^{yy} & \mathcal{A}_i^{yz} \\ \mathcal{A}_i^{zx} & \mathcal{A}_i^{zy} & \mathcal{A}_i^{zz} \end{pmatrix}. \quad (D2)$$

In principle, the elements of this matrix can be measured by Knight-shift experiments, but components of the tensor for different i are related by the crystal symmetries which we use in the following. To derive the effect of the elements of the coupling matrix, we start from the general expression for spin-lattice relaxation rate as

$$\frac{1}{T_1} \propto \int_{-\infty}^{\infty} dt \cos(\omega_0 t) (\langle \{h_x(t), h_x\} + \{h_y(t), h_y\} \rangle), \quad (D3)$$

where h_x and h_y are the x and y components of

$$\mathbf{h} = \sum_i \bar{\mathcal{A}}_i \cdot \mathbf{S}_{i\alpha}. \quad (D4)$$

By performing a Fourier transformation for the electron spins

$$\mathbf{S}_{i\alpha} = \frac{1}{\sqrt{N}} \sum_{\mathbf{q}} e^{i\mathbf{q}\cdot\mathbf{r}_i} \mathbf{S}_{\mathbf{q}\alpha}, \quad (D5)$$

the relaxation rate can be written as

$$\begin{aligned} \frac{1}{T_1} &\propto \int_{-\infty}^{\infty} dt \frac{1}{N} \sum_{\mathbf{q}} \cos(\omega_0 t) \\ &\times \left(\left\langle \left\{ \left[\sum_i \bar{\mathcal{A}}_i \cdot e^{i\mathbf{q}\cdot\mathbf{r}_i} \mathbf{S}_{\mathbf{q}\alpha} \right]^x(t), \left[\sum_j \bar{\mathcal{A}}_j \cdot e^{-i\mathbf{q}\cdot\mathbf{r}_j} \mathbf{S}_{-\mathbf{q}\beta} \right]^x \right\} \right. \right. \\ &\left. \left. + \left\{ \left[\sum_i \bar{\mathcal{A}}_i \cdot e^{i\mathbf{q}\cdot\mathbf{r}_i} \mathbf{S}_{\mathbf{q}\alpha} \right]^y(t), \left[\sum_j \bar{\mathcal{A}}_j \cdot e^{-i\mathbf{q}\cdot\mathbf{r}_j} \mathbf{S}_{-\mathbf{q}\beta} \right]^y \right\} \right\rangle \right). \end{aligned} \quad (D6)$$

If the conducting electrons couple to the nuclear spin on the same site, such as the vanadium atoms in AV_3Sb_5 kagome metals, this expression will reduce to Eq. (4). However, if the conducting electrons are localized on different sites to the nuclear spins, for example the antimony atoms in AV_3Sb_5 , an additional form factor will enter the expression because of the exponential coefficient in the Fourier transformation [72–74]. In fact, in the experiment which measures the spin-lattice relaxation rate of CsV_3Sb_5 in the superconducting state, the measured ones are the antimony atoms which reside on different sites to the active electron degrees of freedom [48]. Thus to directly connect to the experimental setup, an additional form factor should be considered.

To relate coupling matrices to different nearest neighbors, we use that the Hamiltonian of the kagome lattice is invariant under C_6 rotations in the xy plane. The 60° clockwise rotation $\bar{\mathcal{M}}$ in the xy plane can be expressed as

$$\bar{\mathcal{M}} = \begin{pmatrix} \frac{1}{2} & \frac{\sqrt{3}}{2} & 0 \\ -\frac{\sqrt{3}}{2} & \frac{1}{2} & 0 \\ 0 & 0 & 1 \end{pmatrix}. \quad (D7)$$

For simplicity, we assume that the first coupling matrix is a constant 1 in all directions

$$\bar{\mathcal{A}}_1 = \begin{pmatrix} 1 & 1 & 1 \\ 1 & 1 & 1 \\ 1 & 1 & 1 \end{pmatrix}. \quad (D8)$$

To keep the hyperfine Hamiltonian invariant under C_6 rotation, the second coupling matrix should be

$$\bar{\mathcal{A}}_2 = \bar{\mathcal{M}} \bar{\mathcal{A}}_1 \bar{\mathcal{M}}^{-1} = \begin{pmatrix} \frac{2+\sqrt{3}}{2} & -\frac{1}{2} & \frac{1+\sqrt{3}}{2} \\ -\frac{1}{2} & \frac{2-\sqrt{3}}{2} & \frac{1-\sqrt{3}}{2} \\ \frac{1+\sqrt{3}}{2} & \frac{1-\sqrt{3}}{2} & 1 \end{pmatrix}. \quad (D9)$$

Similarly, the other coupling matrices can be derived

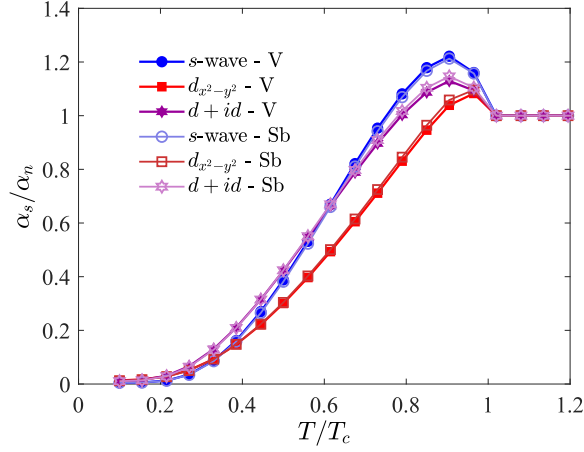


FIG. S4. Comparison of expected spin relaxation rate in a NMR experiment on V nuclear spins and Sb nuclear spins. The temperature dependence of the spin-lattice relaxation rate ratio α_s/α_n exhibits only tiny quantitative differences from the momentum dependent form factors in Eq. (D14). All calculations are done with $\mathcal{N} = 4 \times 10^4$ and $\omega = \eta = 0.015$ and using the Hamiltonian $H_{\text{eff}}(\mathbf{k})$. The solid lines with full symbols correspond to the relaxation rate for the vanadium atoms. The respective lines with open symbols show the results including the form factors, which corresponds to the relaxation rate for the antimony atoms.

$$\bar{\bar{\mathcal{A}}}_3 = \begin{pmatrix} \frac{2-\sqrt{3}}{2} & -\frac{1}{2} & \frac{\sqrt{3}-1}{2} \\ -\frac{1}{2} & \frac{2+\sqrt{3}}{2} & \frac{-1-\sqrt{3}}{2} \\ \frac{\sqrt{3}-1}{2} & \frac{-1-\sqrt{3}}{2} & 1 \end{pmatrix}, \quad (\text{D10})$$

$$\bar{\bar{\mathcal{A}}}_4 = \begin{pmatrix} 1 & 1 & -1 \\ 1 & 1 & -1 \\ -1 & -1 & 1 \end{pmatrix}, \quad (\text{D11})$$

$$\bar{\bar{\mathcal{A}}}_5 = \begin{pmatrix} \frac{2+\sqrt{3}}{2} & -\frac{1}{2} & \frac{-\sqrt{3}-1}{2} \\ -\frac{1}{2} & \frac{2-\sqrt{3}}{2} & \frac{\sqrt{3}-1}{2} \\ \frac{-\sqrt{3}-1}{2} & \frac{\sqrt{3}-1}{2} & 1 \end{pmatrix}, \quad (\text{D12})$$

$$\bar{\bar{\mathcal{A}}}_6 = \begin{pmatrix} \frac{2-\sqrt{3}}{2} & -\frac{1}{2} & \frac{1-\sqrt{3}}{2} \\ -\frac{1}{2} & \frac{2+\sqrt{3}}{2} & \frac{1+\sqrt{3}}{2} \\ \frac{1-\sqrt{3}}{2} & \frac{1+\sqrt{3}}{2} & 1 \end{pmatrix}. \quad (\text{D13})$$

Inserting those coupling matrices into Eq. (D6), we can get the expression of the relaxation rate for antimony atoms

$$\alpha \propto \lim_{\omega \rightarrow 0} \frac{1}{\mathcal{N}} \sum_{\mathbf{q}} \mathcal{F}_{\alpha\beta}(\mathbf{q}) \text{Im} \frac{\chi_{0,\alpha\beta}^{+-}(\mathbf{q}, \omega)}{\omega}, \quad (\text{D14})$$

where the momentum-dependent form factors are given by

$$\mathcal{F}_{AA} = 16 \cos^2 \left(\frac{1}{4} q_x + \frac{\sqrt{3}}{4} q_y \right) + 8 \sin^2 \left(\frac{1}{4} q_x + \frac{\sqrt{3}}{4} q_y \right), \quad (\text{D15})$$

$$\mathcal{F}_{BB} = 16 \cos^2 \left(\frac{1}{2} q_x \right) + 8 \sin^2 \left(\frac{1}{2} q_x \right), \quad (\text{D16})$$

$$\mathcal{F}_{CC} = 16 \cos^2 \left(\frac{1}{4} q_x - \frac{\sqrt{3}}{4} q_y \right) + 8 \sin^2 \left(\frac{1}{4} q_x - \frac{\sqrt{3}}{4} q_y \right), \quad (\text{D17})$$

$$\begin{aligned} \mathcal{F}_{AB} = \mathcal{F}_{BA} = & 4 \cos \left(\frac{1}{4} q_x + \frac{\sqrt{3}}{4} q_y \right) \cos \left(\frac{1}{2} q_x \right) \\ & + 4 \sin \left(\frac{1}{4} q_x + \frac{\sqrt{3}}{4} q_y \right) \sin \left(\frac{1}{2} q_x \right), \end{aligned} \quad (\text{D18})$$

$$\begin{aligned} \mathcal{F}_{BC} = \mathcal{F}_{CB} = & 4 \cos \left(\frac{1}{4} q_x - \frac{\sqrt{3}}{4} q_y \right) \cos \left(\frac{1}{2} q_x \right) \\ & + 4 \sin \left(\frac{1}{4} q_x - \frac{\sqrt{3}}{4} q_y \right) \sin \left(\frac{1}{2} q_x \right), \end{aligned} \quad (\text{D19})$$

$$\begin{aligned} \mathcal{F}_{AC} = \mathcal{F}_{CA} = & 4 \cos \left(\frac{1}{4} q_x + \frac{\sqrt{3}}{4} q_y \right) \cos \left(\frac{1}{4} q_x - \frac{\sqrt{3}}{4} q_y \right) \\ & - 4 \sin \left(\frac{1}{4} q_x + \frac{\sqrt{3}}{4} q_y \right) \sin \left(\frac{1}{4} q_x - \frac{\sqrt{3}}{4} q_y \right). \end{aligned} \quad (\text{D20})$$

Finally, we evaluate Eq. (D14) numerically, to obtain the spin-lattice relaxation rate as expected for the Sb NMR relaxation rate. Figure S4 shows that the form factors do not alter the existence of the Hebel-Slichter peak in the kagome lattice, only small quantitative deviations are visible due the different weighting of the momentum structure of the susceptibility in Eq. (D14). This means that the NMR measurements for the unconventional kagome superconductors with d -wave pairing symmetry are expected to feature the Hebel-Slichter peak, both on vanadium atoms and on antimony atoms.

[1] G. Volovik and L. Gor'kov, Superconducting classes in heavy-fermion systems, JETP **61**, 843 (1985), Zh. Eksp. Teor. Fiz., **88**, 1412, 1985.

[2] M. Sigrist and K. Ueda, Phenomenological theory of unconventional superconductivity, Rev. Mod. Phys. **63**, 239 (1991).

- [3] J. F. Annett, Symmetry of the order parameter for high-temperature superconductivity, *Advances in Physics* **39**, 83 (1990).
- [4] D. J. Scalapino, A common thread: The pairing interaction for unconventional superconductors, *Rev. Mod. Phys.* **84**, 1383 (2012).
- [5] A. Chubukov, Pairing Mechanism in Fe-Based Superconductors, *Annual Review of Condensed Matter Physics* **3**, 57 (2012).
- [6] A. Kreisel, P. J. Hirschfeld, and B. M. Andersen, On the Remarkable Superconductivity of FeSe and Its Close Cousins, *Symmetry* **12**, 1402 (2020).
- [7] A. Kreisel, B. M. Andersen, P. O. Sprau, A. Kostin, J. C. S. Davis, and P. J. Hirschfeld, Orbital selective pairing and gap structures of iron-based superconductors, *Phys. Rev. B* **95**, 174504 (2017).
- [8] A. T. Rømer, D. D. Scherer, I. M. Eremin, P. J. Hirschfeld, and B. M. Andersen, Knight Shift and Leading Superconducting Instability from Spin Fluctuations in Sr_2RuO_4 , *Phys. Rev. Lett.* **123**, 247001 (2019).
- [9] B. R. Ortiz, S. M. L. Teicher, Y. Hu, J. L. Zuo, P. M. Sarte, E. C. Schueller, A. M. M. Abeykoon, M. J. Krogstad, S. Rosenkranz, R. Osborn, R. Seshadri, L. Balents, J. He, and S. D. Wilson, CsV_3Sb_5 : A \mathbb{Z}_2 Topological Kagome Metal with a Superconducting Ground State, *Phys. Rev. Lett.* **125**, 247002 (2020).
- [10] B. R. Ortiz, P. M. Sarte, E. M. Kenney, M. J. Graf, S. M. L. Teicher, R. Seshadri, and S. D. Wilson, Superconductivity in the \mathbb{Z}_2 kagome metal KV_3Sb_5 , *Phys. Rev. Materials* **5**, 034801 (2021).
- [11] Q. Yin, Z. Tu, C. Gong, Y. Fu, S. Yan, and H. Lei, Superconductivity and Normal-State Properties of Kagome Metal RbV_3Sb_5 Single Crystals, *Chin. Phys. Lett.* **38**, 037403 (2021).
- [12] M. L. Kiesel and R. Thomale, Sublattice interference in the kagome Hubbard model, *Phys. Rev. B* **86**, 121105 (2012).
- [13] M. L. Kiesel, C. Platt, and R. Thomale, Unconventional Fermi Surface Instabilities in the Kagome Hubbard Model, *Phys. Rev. Lett.* **110**, 126405 (2013).
- [14] Y.-M. Wu, R. Thomale, and S. Raghu, Sublattice interference promotes pair density wave order in kagome metals, *Phys. Rev. B* **108**, L081117 (2023).
- [15] H. D. Scammell, J. Ingham, T. Li, and O. P. Sushkov, Chiral excitonic order from twofold van Hove singularities in kagome metals, *Nature Communications* **14**, 605 (2023).
- [16] B. R. Ortiz, L. C. Gomes, J. R. Morey, M. Winiarski, M. Bordelon, J. S. Mangum, I. W. H. Oswald, J. A. Rodriguez-Rivera, J. R. Neilson, S. D. Wilson, E. Ertekin, T. M. McQueen, and E. S. Toberer, New kagome prototype materials: discovery of KV_3Sb_5 , RbV_3Sb_5 , and CsV_3Sb_5 , *Phys. Rev. Materials* **3**, 094407 (2019).
- [17] E. M. Kenney, B. R. Ortiz, C. Wang, S. D. Wilson, and M. J. Graf, Absence of local moments in the kagome metal KV_3Sb_5 as determined by muon spin spectroscopy, *J. Phys.: Condens. Matter* **33**, 235801 (2021).
- [18] Y.-X. Jiang, J.-X. Yin, M. M. Denner, N. Shumiya, B. R. Ortiz, G. Xu, Z. Guguchia, J. He, M. S. Hossain, X. Liu, J. Ruff, L. Kautzsch, S. S. Zhang, G. Chang, I. Belopolski, Q. Zhang, T. A. Cochran, D. Multer, M. Litskevich, Z.-J. Cheng, X. P. Yang, Z. Wang, R. Thomale, T. Neupert, S. D. Wilson, and M. Z. Hasan, Unconventional chiral charge order in kagome superconductor KV_3Sb_5 , *Nat. Mater.* **20**, 1353 (2021).
- [19] H. Chen, H. Yang, B. Hu, Z. Zhao, J. Yuan, Y. Xing, G. Qian, Z. Huang, G. Li, Y. Ye, S. Ma, S. Ni, H. Zhang, Q. Yin, C. Gong, Z. Tu, H. Lei, H. Tan, S. Zhou, C. Shen, X. Dong, B. Yan, Z. Wang, and H.-J. Gao, Roton pair density wave in a strong-coupling kagome superconductor, *Nature* **599**, 222 (2021).
- [20] H. Zhao, H. Li, B. R. Ortiz, S. M. L. Teicher, T. Park, M. Ye, Z. Wang, L. Balents, S. D. Wilson, and I. Zeljkovic, Cascade of correlated electron states in the kagome superconductor CsV_3Sb_5 , *Nature* **599**, 216 (2021).
- [21] T. Park, M. Ye, and L. Balents, Electronic instabilities of kagome metals: Saddle points and Landau theory, *Phys. Rev. B* **104**, 035142 (2021).
- [22] Y.-P. Lin and R. M. Nandkishore, Multidome superconductivity in charge density wave kagome metals, *Phys. Rev. B* **106**, L060507 (2022).
- [23] M. M. Denner, R. Thomale, and T. Neupert, Analysis of Charge Order in the Kagome Metal AV_3Sb_5 ($A = \text{K}, \text{Rb}, \text{Cs}$), *Phys. Rev. Lett.* **127**, 217601 (2021).
- [24] R. Tazai, Y. Yamakawa, S. Onari, and H. Kontani, Mechanism of exotic density-wave and beyond-Migdal unconventional superconductivity in kagome metal AV_3Sb_5 ($A = \text{K}, \text{Rb}, \text{Cs}$), *Science Advances* **8**, eabl4108 (2022).
- [25] M. H. Christensen, T. Birol, B. M. Andersen, and R. M. Fernandes, Theory of the charge density wave in AV_3Sb_5 kagome metals, *Phys. Rev. B* **104**, 214513 (2021).
- [26] F. Ferrari, F. Becca, and R. Valentí, Charge density waves in kagome-lattice extended Hubbard models at the van Hove filling, *Phys. Rev. B* **106**, L081107 (2022).
- [27] M. H. Christensen, T. Birol, B. M. Andersen, and R. M. Fernandes, Loop currents in AV_3Sb_5 kagome metals: Multipolar and toroidal magnetic orders, *Phys. Rev. B* **106**, 144504 (2022).
- [28] S.-L. Yu and J.-X. Li, Chiral superconducting phase and chiral spin-density-wave phase in a Hubbard model on the kagome lattice, *Phys. Rev. B* **85**, 144402 (2012).
- [29] W.-S. Wang, Z.-Z. Li, Y.-Y. Xiang, and Q.-H. Wang, Competing electronic orders on kagome lattices at van Hove filling, *Phys. Rev. B* **87**, 115135 (2013).
- [30] X. Wu, T. Schwemmer, T. Müller, A. Consiglio, G. Sangiovanni, D. Di Sante, Y. Iqbal, W. Hanke, A. P. Schnyder, M. M. Denner, M. H. Fischer, T. Neupert, and R. Thomale, Nature of Unconventional Pairing in the Kagome Superconductors AV_3Sb_5 ($A = \text{K}, \text{Rb}, \text{Cs}$), *Phys. Rev. Lett.* **127**, 177001 (2021).
- [31] C. Wen, X. Zhu, Z. Xiao, N. Hao, R. Mondaini, H. Guo, and S. Feng, Superconducting pairing symmetry in the kagome-lattice Hubbard model, *Phys. Rev. B* **105**, 075118 (2022).
- [32] A. T. Rømer, S. Bhattacharyya, R. Valentí, M. H. Christensen, and B. M. Andersen, Superconductivity from repulsive interactions on the kagome lattice, *Phys. Rev. B* **106**, 174514 (2022).
- [33] M.-c. He, H. Zi, H.-x. Zhan, Y.-q. Zhao, C. Ren, X.-y. Hou, L. Shan, Q.-h. Wang, Q. Yin, Z. Tu, C. Gong, H. Lei, Z.-y. Lu, Q. Wang, Y.-p. Qi, G.-f. Chen, and P. Xiong, Strong-coupling superconductivity in the kagome metal CsV_3Sb_5 revealed by soft point-contact spectroscopy, *Phys. Rev. B* **106**, 104510 (2022).
- [34] X.-C. Bai, W.-F. Wu, H.-Y. Wang, Y.-M. Quan, X. Wang, Z. Zeng, and L.-J. Zou, Effective six-band

- model and unconventional spin-singlet pairing in Kagome superconductor CsV_3Sb_5 , *New Journal of Physics* **24**, 123016 (2022).
- [35] J. B. Profe, L. Klebl, F. Grandi, H. Hohmann, M. Dürnagel, T. Schwemmer, R. Thomale, and D. M. Kennes, The kagome Hubbard model from a functional renormalization group perspective, *arXiv e-prints*, arXiv:2402.11916 (2024), arXiv:2402.11916 [cond-mat.str-el].
- [36] X. Wu, D. Chakraborty, A. P. Schnyder, and A. Greco, Crossover between electron-electron and electron-phonon mediated pairing on the kagome lattice, *Phys. Rev. B* **109**, 014517 (2024).
- [37] H. Tan, Y. Liu, Z. Wang, and B. Yan, Charge Density Waves and Electronic Properties of Superconducting Kagome Metals, *Phys. Rev. Lett.* **127**, 046401 (2021).
- [38] J.-F. Zhang, K. Liu, and Z.-Y. Lu, First-principles study of the double-dome superconductivity in the kagome material CsV_3Sb_5 under pressure, *Phys. Rev. B* **104**, 195130 (2021).
- [39] Y. Zhong, S. Li, H. Liu, Y. Dong, K. Aido, Y. Arai, H. Li, W. Zhang, Y. Shi, Z. Wang, S. Shin, H. N. Lee, H. Miao, T. Kondo, and K. Okazaki, Testing electron-phonon coupling for the superconductivity in kagome metal CsV_3Sb_5 , *Nature Communications* **14**, 1945 (2023).
- [40] C. Wang, Y. Jia, Z. Zhang, and J.-H. Cho, Phonon-mediated *s*-wave superconductivity in the kagome metal CsV_3Sb_5 under pressure, *Phys. Rev. B* **108**, L060503 (2023).
- [41] E. T. Ritz, H. S. Røising, M. H. Christensen, T. Birol, B. M. Andersen, and R. M. Fernandes, Superconductivity from orbital-selective electron-phonon coupling in AV_3Sb_5 , *Phys. Rev. B* **108**, L100510 (2023).
- [42] S. D. Wilson and B. R. Ortiz, AV_3Sb_5 kagome superconductors, *Nature Reviews Materials* **9**, 420 (2024).
- [43] Z. Liang, X. Hou, F. Zhang, W. Ma, P. Wu, Z. Zhang, F. Yu, J.-J. Ying, K. Jiang, L. Shan, Z. Wang, and X.-H. Chen, Three-Dimensional Charge Density Wave and Surface-Dependent Vortex-Core States in a Kagome Superconductor CsV_3Sb_5 , *Phys. Rev. X* **11**, 031026 (2021).
- [44] H.-S. Xu, Y.-J. Yan, R. Yin, W. Xia, S. Fang, Z. Chen, Y. Li, W. Yang, Y. Guo, and D.-L. Feng, Multiband Superconductivity with Sign-Preserving Order Parameter in Kagome Superconductor CsV_3Sb_5 , *Phys. Rev. Lett.* **127**, 187004 (2021).
- [45] C. Zhao, L. Wang, W. Xia, Q. Yin, J. Ni, Y. Huang, C. Tu, Z. Tao, Z. Tu, C. Gong, *et al.*, Nodal superconductivity and superconducting domes in the topological Kagome metal CsV_3Sb_5 , *arXiv:2102.08356* (2021).
- [46] Z. Guguchia, C. Mielke, D. Das, R. Gupta, J.-X. Yin, H. Liu, Q. Yin, M. H. Christensen, Z. Tu, C. Gong, N. Shumiya, M. S. Hossain, T. Gamsakhurdashvili, M. Elender, P. Dai, A. Amato, Y. Shi, H. C. Lei, R. M. Fernandes, M. Z. Hasan, H. Luetkens, and R. Khasanov, Tunable unconventional kagome superconductivity in charge ordered RbV_3Sb_5 and KV_3Sb_5 , *Nature Communications* **14**, 153 (2023).
- [47] C. Mielke, D. Das, J.-X. Yin, H. Liu, R. Gupta, Y.-X. Jiang, M. Medarde, X. Wu, H. C. Lei, J. Chang, P. Dai, Q. Si, H. Miao, R. Thomale, T. Neupert, Y. Shi, R. Khasanov, M. Z. Hasan, H. Luetkens, and Z. Guguchia, Time-reversal symmetry-breaking charge order in a kagome superconductor, *Nature* **602**, 245 (2022).
- [48] C. Mu, Q. Yin, Z. Tu, C. Gong, H. Lei, Z. Li, and J. Luo, *S*-Wave Superconductivity in Kagome Metal CsV_3Sb_5 Revealed by $^{121/123}\text{Sb}$ NQR and ^{51}V NMR Measurements, *Chin. Phys. Lett.* **38**, 077402 (2021).
- [49] Y. Zhong, J. Liu, X. Wu, Z. Guguchia, J.-X. Yin, A. Mine, Y. Li, S. Najafzadeh, D. Das, C. Mielke, R. Khasanov, H. Luetkens, T. Suzuki, K. Liu, X. Han, T. Kondo, J. Hu, S. Shin, Z. Wang, X. Shi, Y. Yao, and K. Okazaki, Nodeless electron pairing in CsV_3Sb_5 -derived kagome superconductors, *Nature* **617**, 488 (2023).
- [50] W. Duan, Z. Nie, S. Luo, F. Yu, B. R. Ortiz, L. Yin, H. Su, F. Du, A. Wang, Y. Chen, X. Lu, J. Ying, S. D. Wilson, X. Chen, Y. Song, and H. Yuan, Nodeless superconductivity in the kagome metal CsV_3Sb_5 , *Sci. China: Phys. Mech. Astron.* **64**, 107462 (2021).
- [51] R. Gupta, D. Das, C. H. Mielke III, Z. Guguchia, T. Shiroka, C. Baines, M. Bartkowiak, H. Luetkens, R. Khasanov, Q. Yin, Z. Tu, C. Gong, and H. Lei, Microscopic evidence for anisotropic multigap superconductivity in the CsV_3Sb_5 kagome superconductor, *npj Quantum Mater.* **7**, 49 (2022).
- [52] M. Roppongi, K. Ishihara, Y. Tanaka, K. Ogawa, K. Okada, S. Liu, K. Mukasa, Y. Mizukami, Y. Uwamoto, R. Grasset, M. Konczykowski, B. R. Ortiz, S. D. Wilson, K. Hashimoto, and T. Shibauchi, Bulk evidence of anisotropic *s*-wave pairing with no sign change in the kagome superconductor CsV_3Sb_5 , *Nature Communications* **14**, 667 (2023).
- [53] R. Gupta, D. Das, C. Mielke, E. T. Ritz, F. Hotz, Q. Yin, Z. Tu, C. Gong, H. Lei, T. Birol, R. M. Fernandes, Z. Guguchia, H. Luetkens, and R. Khasanov, Two types of charge order with distinct interplay with superconductivity in the kagome material CsV_3Sb_5 , *Commun. Phys.* **5**, 232 (2022).
- [54] W. Zhang, X. Liu, L. Wang, C. W. Tsang, Z. Wang, S. T. Lam, W. Wang, J. Xie, X. Zhou, Y. Zhao, S. Wang, J. Tallon, K. T. Lai, and S. K. Goh, Nodeless Superconductivity in Kagome Metal CsV_3Sb_5 with and without Time Reversal Symmetry Breaking, *Nano Letters* **23**, 872 (2023).
- [55] A. V. Balatsky, I. Vekhter, and J.-X. Zhu, Impurity-induced states in conventional and unconventional superconductors, *Rev. Mod. Phys.* **78**, 373 (2006).
- [56] M. N. Gastiasoro, F. Bernardini, and B. M. Andersen, Unconventional Disorder Effects in Correlated Superconductors, *Phys. Rev. Lett.* **117**, 257002 (2016).
- [57] M. N. Gastiasoro and B. M. Andersen, Enhancing superconductivity by disorder, *Phys. Rev. B* **98**, 184510 (2018).
- [58] A. T. Rømer, P. J. Hirschfeld, and B. M. Andersen, Raising the Critical Temperature by Disorder in Unconventional Superconductors Mediated by Spin Fluctuations, *Phys. Rev. Lett.* **121**, 027002 (2018).
- [59] B. M. Andersen, A. Kreisel, and P. J. Hirschfeld, Spontaneous time-reversal symmetry breaking by disorder in superconductors, *Front. Phys.* **12**, 1353425 (2024).
- [60] S. C. Holbæk, M. H. Christensen, A. Kreisel, and B. M. Andersen, Unconventional superconductivity protected from disorder on the kagome lattice, *Phys. Rev. B* **108**, 144508 (2023).
- [61] J. Rossat-Mignod, L. Regnault, G. Vettier, P. Bourges, P. Burlet, J. Bossy, J. Henry, and G. Lapertot, Neutron scattering study of the $\text{YBa}_2\text{Cu}_3\text{O}_{6+x}$ system, *Physica*

- C: Superconductivity **185-189**, 86 (1991).
- [62] H. A. Mook, M. Yethiraj, G. Aeppli, T. E. Mason, and T. Armstrong, Polarized neutron determination of the magnetic excitations in $\text{YBa}_2\text{Cu}_3\text{O}_7$, *Phys. Rev. Lett.* **70**, 3490 (1993).
 - [63] A. D. Christianson, E. A. Goremychkin, R. Osborn, S. Rosenkranz, M. D. Lumsden, C. D. Malliakas, I. S. Todorov, H. Claus, D. Y. Chung, M. G. Kanatzidis, R. I. Bewley, and T. Guidi, Unconventional superconductivity in $\text{Ba}_{0.6}\text{K}_{0.4}\text{Fe}_2\text{As}_2$ from inelastic neutron scattering, *Nature* **456**, 930 (2008).
 - [64] D. S. Inosov, J. T. Park, P. Bourges, D. L. Sun, Y. Sidis, A. Schneidewind, K. Hradil, D. Haug, C. T. Lin, B. Keimer, and V. Hinkov, Normal-state spin dynamics and temperature-dependent spin-resonance energy in optimally doped $\text{BaFe}_{1.85}\text{Co}_{0.15}\text{As}_2$, *Nature Physics* **6**, 178 (2010).
 - [65] C. Stock, C. Broholm, J. Hudis, H. J. Kang, and C. Petrovic, Spin Resonance in the d -Wave Superconductor CeCoIn_5 , *Phys. Rev. Lett.* **100**, 087001 (2008).
 - [66] T. Moriya, The effect of electron-electron interaction on the nuclear spin relaxation in metals, *Journal of the Physical Society of Japan* **18**, 516 (1963).
 - [67] F. Hammerath, *Magnetism and Superconductivity in Iron-based Superconductors as Probed by Nuclear Magnetic Resonance* (Springer Spektrum, 2012).
 - [68] M. Tinkham, *Introduction to superconductivity* (McGraw-Hill New York, 1975).
 - [69] D. Parker and S. Haas, T_1^{-1} peak near T_c in unconventional Bardeen-Cooper-Schrieffer superconductors, *Phys. Rev. B* **75**, 052501 (2007).
 - [70] J. Liu and T. Zhou, Probing the pairing symmetry in kagome superconductors based on the single-particle spectrum, *Phys. Rev. B* **109**, 054504 (2024).
 - [71] S. Sumita, M. Naka, and H. Seo, Fulde-Ferrell-Larkin-Ovchinnikov state induced by antiferromagnetic order in κ -type organic conductors, *Phys. Rev. Res.* **5**, 043171 (2023).
 - [72] A. Smerald and N. Shannon, Angle-resolved NMR: Quantitative theory of ^{75}As T_1 relaxation rate in BaFe_2As_2 , *Phys. Rev. B* **84**, 184437 (2011).
 - [73] B. S. Shastry, t-J model and nuclear magnetic relaxation in high- T_c materials, *Phys. Rev. Lett.* **63**, 1288 (1989).
 - [74] F. Mila and T. M. Rice, Spin dynamics of $\text{YBa}_2\text{Cu}_3\text{O}_{6+x}$ as revealed by NMR, *Phys. Rev. B* **40**, 11382 (1989).